Active System To Generate Views Of Facial Features With Selectable Resolution

Arnd Gebhard* and Dietrich Paulus*

University of Erlangen, Chair for Pattern Recognition
Martensstrasse 3, D-91058 Erlangen, Germany
Email: gebhard@informatik.uni-erlangen.de

Abstract

In many applications concerning the analysis of a human face or of facial features, images with selectable resolutions are desirable. The first step of our system is the detection of facial features. We present a parametric face model for localization and evaluate the model by an energy minimization process.

To change the resolution selected by the user, we need a camera with a calibrated zooming unit. We present a method to calibrate the zoom unit of a camera with pan/tilt unit. The advantage of the approach is that the focal length can be related to the stepper motor setting without any calibration pattern or knowledge about the scene.

1 Introduction

The processing of face images receives more and more attention in the field of image analysis. There are many different problems and applications which base on the processing of such images. The tasks of facial image analysis include the face localization [15, 9], the recognition of human faces [12, 2, 13], and the analysis of mimics or facial expressions [16, 10, 14]. Applications exist, for instance, for access control of rooms and buildings [5, 7], the indexing of police mugshots [3] or medical tasks [1]. Another important application results from object–based image coding and transmission[6, 8].

The analysis of facial features often utilizes information about subtle structures inside the face. It is often helpful to get views of faces and facial features with determined resolutions. Much more information about a facial feature can be included in a zoomed view, than in a view of the whole head. For this purpose we developed an active system to generate such views.

The following steps are perfomed while generating a view: A face and the facial features are localized in an image. The camera performs pan and tilt movements to center the requested facial feature. A necessary change of the zoom status is calculated by means of the actual and the user selected resolution of the facial feature. For the pan and tilt movements and the change of the zoom status it is necessary to know the relation between the incremental status of the zoom unit and the focal length of the camera.

The organization of this contribution is as follows: The localization of faces and facial features will be described in detail in Sect. 2. An approach to calibrate the focal length of the camera will be shown in Sect. 3. The single components are combined to an active system which is described in Sect. 4. Results are shown in Sect. 5. Finally Sect. 6 summarizes the contribution and the main results.

*partially funded by DFG, SFB 603 TP B3

2 Localization of Faces and Facial Features

In our system the localization of faces and facial features is a model–driven energy–minimization process. For that four sequential optimizations are computed. In the following section we present the parametric face model and describe the optimization process for the parameter calculation.

2.1 Face Model

We assume that the patient's face is the dominant region inside the image. The background is expected either to be homogeneous or a background image is captured prior to the analysis which is used to part foreground from background. The localization is executed by calculating parameters of the face model shown in Figure 1. All calculations are performed on the edge strength part $\boldsymbol{f}_{\mathrm{s}}$ of a Sobel filtered image $\boldsymbol{f}$. In the following N_{x} denotes the horizontal size of the image and N_{y} denotes the vertical image size.

2.2 Localization

The *first* step is to localize the upper arc of the face. A ring segment with fixed width C_{R} is found in the image which is expected to be the top of the patient's head.

There are three parameters which have to be estimated: the x–coordinate x_{h} and the y–coordinate y_{h} of the origin $\boldsymbol{q}_{\mathrm{h}}$ and the radius R_{h} of the arc. We expect much edge energy between patient and background. That lets us find the parameters of the circle and of the following part of the model in the edge strength representation of the original image.

The following equation gives the edge–energy inside the head arc in the image:

$$E_{\mathrm{h}} = \int_{0}^{\pi} \int_{R_{\mathrm{h}}}^{R_{\mathrm{h}}+C_{\mathrm{R}}} \boldsymbol{f}_{\mathrm{s}}(x_{\mathrm{h}} + r\cos\phi, \; y_{\mathrm{h}} + r\sin\phi)\, dr\, d\phi \qquad (1)$$

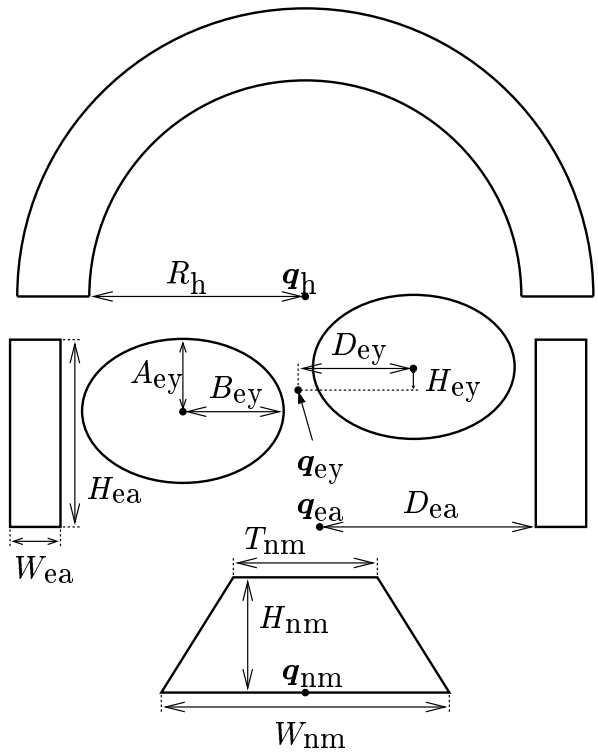

Figure 1: Parametric Face Model. All shown parameters are optimized during face localization.

The minimization process has to determine the optimal parameters

$$\left(x_{\mathrm{h}}{}^{*}, y_{\mathrm{h}}{}^{*}, R_{\mathrm{h}}{}^{*}\right) = \underset{(x_{\mathrm{h}}, y_{\mathrm{h}}, R_{\mathrm{h}})}{\operatorname{argmax}} \frac{E_{\mathrm{h}}}{\left(\frac{(R_{\mathrm{h}}+C_{\mathrm{R}})^2 - R_{\mathrm{h}}{}^2}{2}\right)^{C_{\mathrm{h}}}} \qquad (2)$$

The expression (2) optimizes the ratio of edge energy to surface for the head arc. C_{h} is a constant which influences this ratio. The values of the constants are $C_{\mathrm{R}} = 20$ and $C_{\mathrm{h}} = 1.4$.

The optimization is performed by an adaptive random search whith a subsequent local simplex method[4]. To speed up the optimization there are restrictions for plausible parameters: The parameter x_{h} can vary form $N_{\mathrm{x}}/4$ to $3\,N_{\mathrm{x}}/4$, y_{h} form $N_{\mathrm{y}}/4$ to $N_{\mathrm{y}}/2$, and R_{h} from $N_{\mathrm{x}}/10$ to $N_{\mathrm{x}}/3$.

The *next* step is to localize the ears which are modeled as rectangles positioned below the arc of the head. The parameters which have to be determined are the position of the origin $\boldsymbol{q}_{\mathrm{ea}}$, the width W_{ea} and height H_{ea} of

the ears, and the distance $2D_{\mathrm{ea}}$ between the two ears.
The equation to calculate the edge–energy is

$$E_{\mathrm{ea}} = \int_0^{W_{\mathrm{ea}}} \int_0^{H_{\mathrm{ea}}} \boldsymbol{f}_{\mathrm{s}}(x_{\mathrm{ea}} + w + D_{\mathrm{ea}}, y_{\mathrm{ea}} + h)$$

$$+\boldsymbol{f}_{\mathrm{s}}(x_{\mathrm{ea}} + w - D_{\mathrm{ea}}, y_{\mathrm{ea}} + h)\, dh\, dw \qquad (3)$$

and the optimal values can be determined as

$$(x_{\mathrm{ea}}{}^*, y_{\mathrm{ea}}{}^*, D_{\mathrm{ea}}{}^*, W_{\mathrm{ea}}{}^*, H_{\mathrm{ea}}{}^*) =$$

$$\underset{(x_{\mathrm{ea}}, y_{\mathrm{ea}}, D_{\mathrm{ea}}, W_{\mathrm{ea}}, H_{\mathrm{ea}})}{\operatorname{argmax}} \frac{(E_{\mathrm{ea}}\, D_{\mathrm{ea}})^{C_{\mathrm{ea}}}}{(W_{\mathrm{ea}}\, H_{\mathrm{ea}})} \qquad (4)$$

with constant $C_{\mathrm{ea}} = 1.4$ which influences the ratio of energy to surface for the ears.

There are anatomic restrictions for the ear parameters. The origin of the ears $\boldsymbol{q}_{\mathrm{ea}}$ must have a lower horizontal distance than $R_{\mathrm{h}}/3$, the vertical position of $\boldsymbol{q}_{\mathrm{ea}}$ must be below the origin of the head arc $\boldsymbol{q}_{\mathrm{h}}$, but with a lower distance than $R_{\mathrm{h}}/2$. D_{ea} must be between $0.9R_{\mathrm{h}}$ and $N_{\mathrm{x}}/3$.

The eyes, which are found in the *third* step, are modeled as ellipses. The parameter $\boldsymbol{q}_{\mathrm{ey}} = \left(x_{\mathrm{ey}}, y_{\mathrm{ey}}\right)^{\mathrm{T}}$ is the position of the origin of the eyes, A_{ey} and B_{ey} the length of the ellipses axis, $2H_{\mathrm{ey}}$ the vertical and $2D_{\mathrm{ey}}$ the horizontal distance of the eye centers to each other. We use the following equation to localize them:

$$E_{\mathrm{ey}} = \int_0^{2\pi} \int_0^{1} \boldsymbol{f}_{\mathrm{s}}(x_{\mathrm{ey}} + A_{\mathrm{ey}} r \cos\phi + D_{\mathrm{ey}},$$

$$y_{\mathrm{ey}} + B_{\mathrm{ey}} r \sin\phi + H_{\mathrm{ey}}) +$$

$$+\boldsymbol{f}_{\mathrm{s}}(x_{\mathrm{ey}} + A_{\mathrm{ey}} r \cos\phi - D_{\mathrm{ey}},$$

$$y_{\mathrm{ey}} + B_{\mathrm{ey}} r \sin\phi - H_{\mathrm{ey}})\, dr\, d\phi \qquad (5)$$

With the following optimization we get the eye parameters:

$$\left(x_{\mathrm{ey}}{}^*, y_{\mathrm{ey}}{}^*, D_{\mathrm{ey}}{}^*, A_{\mathrm{ey}}{}^*, B_{\mathrm{ey}}{}^*, H_{\mathrm{ey}}{}^*\right) =$$

$$\underset{(x_{\mathrm{ey}}, y_{\mathrm{ey}}, D_{\mathrm{ey}}, A_{\mathrm{ey}}, B_{\mathrm{ey}})}{\operatorname{argmax}} \frac{E_{\mathrm{ey}}}{\left(\frac{A_{\mathrm{ey}}{}^2 + B_{\mathrm{ey}}{}^2}{4}\pi\right)^{C_{\mathrm{ey}}}} \qquad (6)$$

with a constant $C_{\mathrm{ey}} = 1.4$ influencing the ratio of energy to surface for the eyes.

The anatomic restrictions here are: The horizontal distance of the origin of the eyes $\boldsymbol{q}_{\mathrm{ey}}$ must be less than $R_{\mathrm{h}}/3$, the vertical position must be greater than y_{h} but lower than $y_{\mathrm{h}} + R_{\mathrm{h}}$. A_{ey} and B_{ey} must be lower than $0.4R_{\mathrm{h}}$ and D_{ey} lower than D_{ea}. The two eye regions must not overlap and the eye regions must not overlap the ears' regions.

Finally the nose/mouth region is to be found. It is modeled as a triangle stump with parameters origin $\boldsymbol{q}_{\mathrm{nm}} = (x_{\mathrm{nm}}, y_{\mathrm{nm}})^T$, height H_{nm}, length of base line W_{nm} and the ratio R_{nm} of length of base line to length of top line. In Figure 1 we defined a parameter T_{nm} as the length of the top line.

The amount of edge strength in the nose mouth region can be determined by the following equation:

$$E_{\mathrm{nm}} = \int_0^{H_{\mathrm{nm}}} \int_{-1}^{1} \boldsymbol{f}_{\mathrm{s}}(x_{\mathrm{nm}} + w\,(W_{\mathrm{nm}} - \frac{h}{H_{\mathrm{nm}}}$$

$$(W_{\mathrm{nm}} - T_{\mathrm{nm}})), y_{\mathrm{nm}} + h)\, dw\, dh \qquad (7)$$

The optimal parameters are found as

$$(x_{\mathrm{nm}}{}^*, y_{\mathrm{nm}}{}^*, W_{\mathrm{nm}}{}^*, T_{\mathrm{nm}}{}^*, H_{\mathrm{nm}}{}^*) =$$

$$\underset{\substack{(x_{\mathrm{nm}}, y_{\mathrm{nm}},\\ W_{\mathrm{nm}}, T_{\mathrm{nm}}, H_{\mathrm{nm}})}}{\operatorname{argmax}} \frac{(E_{\mathrm{nm}})^{C_{\mathrm{nm}}}}{(W_{\mathrm{nm}} + T_{\mathrm{nm}})\, H_{\mathrm{nm}}{}^2} \qquad (8)$$

here with the constant $C_{\mathrm{nm}} = 1.2$.

The horizontal distance of the origin $\boldsymbol{q}_{\mathrm{nm}}$ must be lower than $D_{\mathrm{ey}}/3$ from $\boldsymbol{q}_{\mathrm{ey}}$. The vertical position must be between $y_{\mathrm{ey}} + 2D_{\mathrm{ey}}$ and $y_{\mathrm{ey}} + 3D_{\mathrm{ey}}$. W_{nm} must be between $2D_{\mathrm{ey}}$ and $3D_{\mathrm{ey}}$, T_{nm} between D_{ey} and $2D_{\mathrm{ey}}$, and H_{nm} between D_{ey} and $3D_{\mathrm{ey}}$.

All the restrictions to the optimized parameters were imposed because of observations of anatomic facts. The constants C_{R}, C_{h}, C_{ea}, C_{ey}, and C_{nm} which were used for the calculations were determined experimentally by localization and tracking of patient faces and facial features in 1000 images.

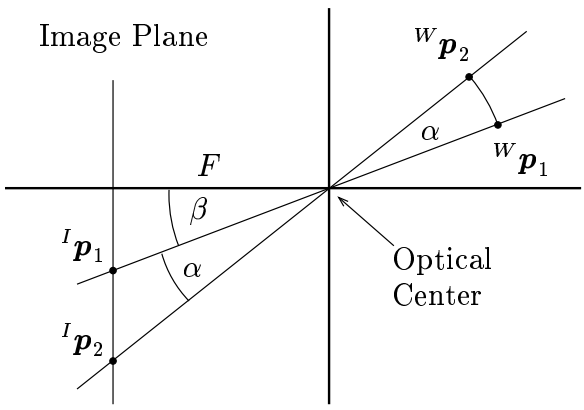

Figure 2: View of Calibration scene from the side whith image plane projected to a line

3 Calibration of a Camera's Zoom Unit

In this section we present a method to calibrate the zoom unit of a camera. The result will be the a graph that implies the dependency of the focal length of the camera to the increment status of the zoom unit.

The calibration bases on the fact that, if the viewing direction of a camera is changed by a camera rotation around the opical center, the image points are displaced, and that the displacement increases when the focal length increases.

3.1 Calibration Equation

In Figure 2 the parameters for the calibration are shown. A point $^W\boldsymbol{p}_1$ in the world is mapped to the image point $^I\boldsymbol{p}_1$. After a camera rotation of angle α around the optical center, which can also be interpreted as the rotation of $^W\boldsymbol{p}_1$ to the point $^W\boldsymbol{p}_2$ with angle $-\alpha$, the result is $^I\boldsymbol{p}_2$. We calculate the focal length F of the camera from the camera rotation angle α and the image points $^W\boldsymbol{p}_1$ and $^W\boldsymbol{p}_2$. The tracking is done with the approach presented in [11].

The segmented points $^I\boldsymbol{p}_1$ and $^I\boldsymbol{p}_2$ are first translated orthogonally to the direction of line $^I\boldsymbol{p}_1 + \lambda(^I\boldsymbol{p}_2 - {}^I\boldsymbol{p}_1)$ to the points $^I\boldsymbol{p}'_1 = ({}^I_xp'_1, {}^I_yp'_1)^{\mathrm{T}}$ and $^I\boldsymbol{p}'_2 = ({}^I_xp'_2, {}^I_yp'_2)^{\mathrm{T}}$ such that the elongation of line $^I\boldsymbol{p}'_1 + \lambda(^I\boldsymbol{p}'_2 - {}^I\boldsymbol{p}'_1)$ crosses the

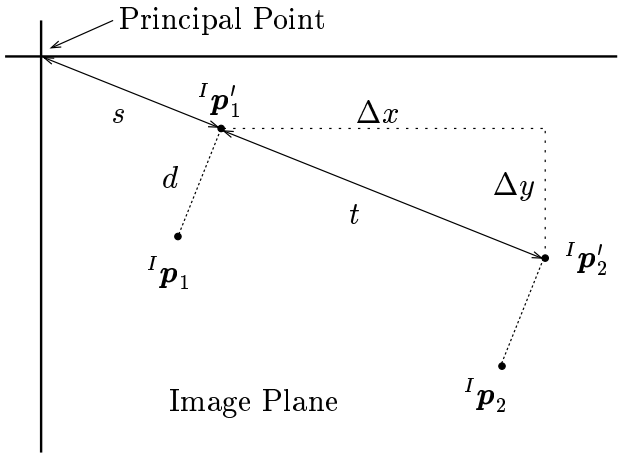

Figure 3: View of Calibration scene. Viewing direction parallel camera viewing direction.

principal point (Figure 3). Under the assumption of a pinhole camera all image points lying on the extension of the line $^I\boldsymbol{p}_1 + \lambda(^I\boldsymbol{p}'_1 - {}^I\boldsymbol{p}_1)$ will be transferred for the same distance t when the camera is rotated by an angle α.

In the following we determine all the parameters of Figure 3 which are used for the zoom calibration.

$$\Delta x := |{}^I_xp_1 - {}^I_xp_2| = |{}^I_xp'_1 - {}^I_xp'_2| \tag{9}$$

$$\Delta y := |{}^I_yp_1 - {}^I_yp_2| = |{}^I_yp'_1 - {}^I_yp'_2| \tag{10}$$

$$d = \frac{{}^I_yp_2 - {}^I_yp_1}{\sqrt{\Delta x^2 + \Delta y^2}}\,{}^I_xp_1 - \frac{{}^I_xp_1 - {}^I_xp_2}{\sqrt{\Delta x^2 + \Delta y^2}}\,{}^I_yp_1 \tag{11}$$

$$s = \sqrt{{}^I_xp_1{}^2 + {}^I_xp_1{}^2 - d^2} \tag{12}$$

$$t = \sqrt{(\Delta x)^2 + (\Delta y)^2} \tag{13}$$

From Figure 2 and Figure 3 the following equations can be derived:

$$\beta = \arctan\left(\frac{s}{F}\right) \tag{14}$$

$$\alpha + \beta = \arctan\left(\frac{s+t}{F}\right) \tag{15}$$

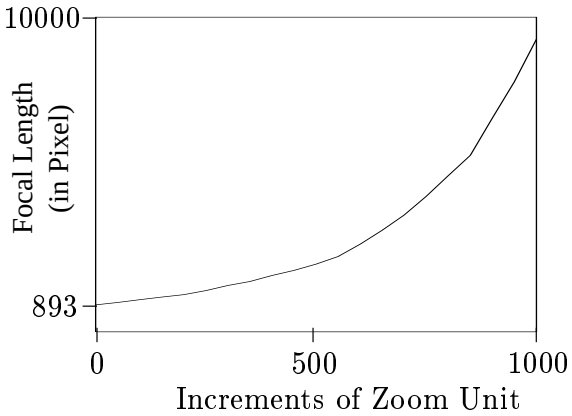

Figure 4: Result of Zoom Calibration

The substraction of (15) − (14) gives

$$\begin{aligned} \alpha &= \arctan\left(\frac{s+t}{F}\right) - \arctan\left(\frac{s}{F}\right) \\ &= \arctan\left(\frac{\frac{t}{F}}{1+\frac{s(s+t)}{F^2}}\right) \end{aligned} \tag{16}$$

and a closed solution for F can be given:

$$F = \frac{1}{2\tan(\alpha)}\left(t + \sqrt{t^2 - 4s(s+t)\tan(\alpha)^2}\right) \tag{17}$$

This formula was used to calculated the focal length of a Sony EVI D31 camera depending on the status of the zoom unit. In Figure 4 the graph of the resulting function is shown.

One assumption we made was that the camera's rotation center is the optical center of the camera. This assumption not valid in reality. In the next section we will consider this problem.

3.2 Sensibility

The positions of the optical center $\boldsymbol{q}_{\mathrm{O}}$ of the camera and of the center of the camera rotation $\boldsymbol{q}_{\mathrm{r}}$ differ in reality. This difference influences the quality of the calibration of the zoom unit. The error resulting from this fact will be quantified in the following.

In Figure 2 the case of a rotation center equal to an optical center is shown. In Figure 5 the camera rotation center $\boldsymbol{q}_{\mathrm{r}}$ and the optical center $\boldsymbol{q}_{\mathrm{O}}$ differ. The error–free case

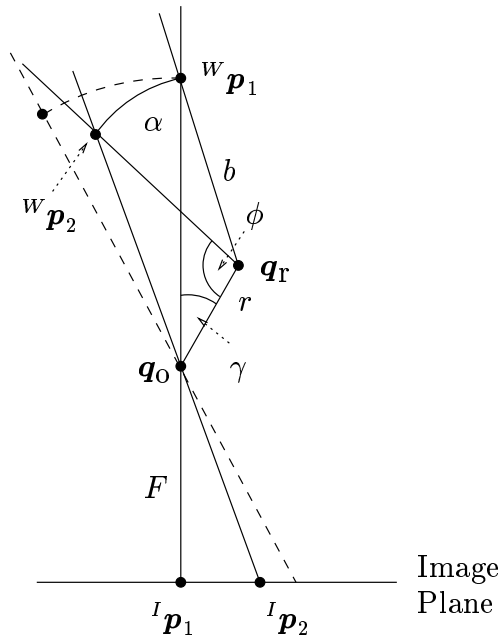

Figure 5: Optical center and rotation center at different positions

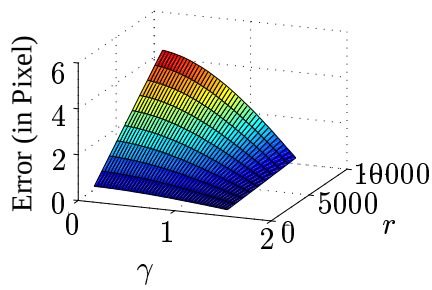

Figure 6: Variation of displacement

is shown as dashed lines. The difference of the image point $^I\boldsymbol{p}_2$ and the projection in the error–free case is obvious.

The image point ${}^I_x p_2$ can be calculated with the formula

$${}^I_x p_2 = F\ \tan(\gamma - \arcsin(\frac{b\,sin\phi}{\sqrt{r^2+b^2-2rb\cos\phi}})) \tag{18}$$

The graph of the relation of the displacement to r and γ is shown in Figure 6. The focal length is kept constant (1000 pixels), as well as the distance b between optical center and object point (200 000 pixel) and α (5 degree). At a radius of 10000 pixels the distance varies by maximally 4.3 pixels or a maximal error of 5%. That also yields a maximal error of the focal length of 5%.

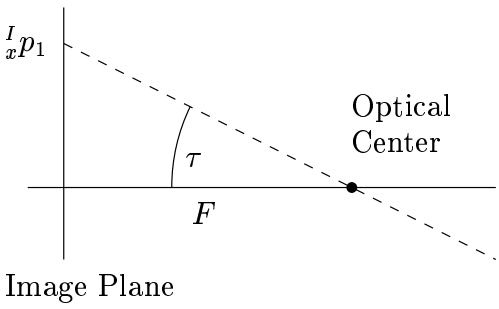

Figure 7: Parameters for the calculation of the pan angle

4 Active System

With the presented modules we implemented an active system for the generation of face and facial feature views. The zoom calibration has to be executed. The starting point is a person sitting in front of the system. With the information which facial feature to record and the desired resolution, the views can be generated.

First, a image with a relative short focal length is generated. All persons for whom the recording is done, sit in approximatelly the same distance to the camera. That makes it easy to determine a focal length for which the whole face fits into the image and appears as the dominant region.

The face is localized by optimizing the model parameter as described in Sect. 2. The result are the center of the eyes $\boldsymbol{q}_{\mathrm{re}} = (x_{\mathrm{ey}} - D_{\mathrm{ey}}, y_{\mathrm{ey}} - H_{\mathrm{ey}})^{\mathrm{T}}$ and $\boldsymbol{q}_{\mathrm{le}} = (x_{\mathrm{ey}} + D_{\mathrm{ey}}, y_{\mathrm{ey}} + H_{\mathrm{ey}})^{\mathrm{T}}$ and the center of the mouth $\boldsymbol{q}_{\mathrm{nm}}$.

The center of the current facial feature has to be translated to the center of the image. This is done by rotation of the pan and tilt axis of the camera. We assume that a movement of the pan axis will produce a translation of the image points in x–direction, and a movement of the tilt axis yields a translation in y–direction. In Figure 7 the calculation parameters for the pan axis are shown. The following equation for the pan axis arises:

$$\tau = \arctan(\frac{{}^{I}_{x}p_1}{F}) \tag{19}$$

Head	95%
Ears	95%
Eyes	82%
Nose/Mouth	73%

Table 1: Results of the localization of human faces and facial features

Figure 8: Face as the dominant image region

and in analogy the equation for the tilt axis:

$$\sigma = \arctan(\frac{{}^{I}_{y}p_1}{F}) \tag{20}$$

In contrast to the zoom stepper motor, the pan/tilt motors exhibit a linear relation to the rotation angles.

The resolution of the current facial feature is specified in pixels. The new number of pixels for the width of the mouth $W_{\mathrm{nm}}{}'$ or the diameter of the eye $2\,A_{\mathrm{ey}}{}'$ has to be determined. The new focal length is calculated as

$$F' = F\,\frac{A_{\mathrm{ey}}}{A_{\mathrm{ey}}{}'} \quad \text{or} \quad F' = F\,\frac{W_{\mathrm{nm}}}{W_{\mathrm{nm}}{}'} \tag{21}$$

and transferred to zoom unit increments by means of the zoom calibration result.

In the next section we show results which we obtained while evaluating the system.

5 Experiments

The localization of human faces in images is performed by a parametric face model (Sect. 2). The rates of correct localization of faces and facial features are presented in Table 1. Every simplex–optimization for the

Head: $(x_{\mathrm{h}}{}^*, y_{\mathrm{h}}{}^*, R_{\mathrm{h}}{}^*)$	(191,123,65)
Ears: $(x_{\mathrm{ea}}{}^*, y_{\mathrm{ea}}{}^*, D_{\mathrm{ea}}{}^*, W_{\mathrm{ea}}{}^*, H_{\mathrm{ea}}{}^*)$	(192,144,20,62,93)
Eyes: $(x_{\mathrm{ey}}{}^*, y_{\mathrm{ey}}{}^*, D_{\mathrm{ey}}{}^*, A_{\mathrm{ey}}{}^*, B_{\mathrm{ey}}{}^*, H_{\mathrm{ey}}{}^*)$	(194, 153, 31, 26, 22, 1)
Nose/Mouth: $(x_{\mathrm{nm}}{}^*, y_{\mathrm{nm}}{}^*, W_{\mathrm{nm}}{}^*, T_{\mathrm{nm}}{}^*, H_{\mathrm{nm}}{}^*)$	(190,229, 63, 31, 43)

Table 2: Computed parameters (see Figure 1) for the real face in Figure 8

Figure 9: Localization results

Figure 10: Left eye in determined resolution

head, the ears, the eyes, and the nose/mouth regions are initialized with 5000 parameter sets. The best 200 are then used for the local downhill optimization. The calculation times for the localization are approximatelly 40 seconds per frame.

A human face is the dominant region in Figure 8. The image was generated with a focal length of 1022 pixel ($\approx$ 8.4mm). The localization results are shown graphically in Figure 9 and numerically in Table 2. The system was directed to generate views of the left eye with diameter 300 pixels (Figure 10) and of the mouth with diameter 100 pixel (Figure 11). The average measured zoom error is less than 5% and the average position error less than 10 pixel.

Figure 11: Mouth in determined resolution

6 Conclusion

We presented an active system for the generation of views of human face features with a selectable resolution. Several different steps were necessary:

For the localization of faces and facial features we introduced a parametric model and fitted it with an energy minimization method to the image data. With the face model, the localization of face features can be performed with a recognition rate of 82% for the eyes and 73% for the nose–mouth region.

We presented a calibration method for a zoom unit of a camera. The calibration bases on the observation that image points are translated when the pan or tilt axis of a camera is changed by a rotation. The larger the focal length of the camera is, the bigger is the translation of the image points. The assumption that the positions of rotation axis of pan and tilt camera motions crosses the optical center of the camera is not valid in reality. This fact yields a systematic calibration error less than 5% of the total focal length.

The active system combines all the presented modules. A view of a human face is recorded. The face and the facial features are localized. The angles of the pan and tilt units

and the increments of the zoom unit are calculated and transferred to the camera controller to generate views of facial features with the determined resolution.

The system is part of a medical application for the automatic diagnosis support of facial paralysis.

Bibliography

1. U. Ahlrichs, D. Paulus, and S. Wolf. Objektivierung der Beurteilung von Gesichtsasymmetrien durch Bildanalyse. In T. Lehmann, I. Scholl, and K. Spitzer, editors, *Workshop Bildverarbeitung für die Medizin*, pages 125–130, Aachen, 1996.
2. R. Brunelli and T. Poggio. Face recognition: Features versus templates. *IEEE Transactions on Pattern Analysis and Machine Intelligence*, 15(10):1042–1052, 1993.
3. Ian Craw, David Tock, and Alan Bennett. Finding face features. In G. Sandini, editor, *Computer Vision — ECCV '92*, Lecture Notes in Computer Science, pages 92–96, Santa Margherita Ligure, 1992. Springer.
4. S. M. Ermakov and A. A. Zhiglyavskij. On random search of global extremum. *Probability Theory and Applications*, 28(1):129–136, 1983.
5. W. Konen and E. Schulze-Krüger. ZN-face: A system for access control using automated face recognition. In *Proceedings of the International Workshop on Automatic Face and Gesture Recognition*, pages 18–24, Zürich, 1995.
6. H. Li, P. Roivainen, and R. Forchheimer. 3D motion estimation in model-based image coding. *IEEE Transactions on Pattern Analysis and Machine Intelligence*, 15(6):545–555, June 1993.
7. S.J. McKenna and S. Gong. Non-intrusive person authentication for access control by visual tracking and face recognition. In *International Conference on Audio- and Video-Based Biometric Person Authentication*, volume 1206 of *Lecture Notes in Computer Science*, pages 177–184. Springer Verlag, March 1997.
8. B. Moghaddam and A. Pentland. An automatic system for model-based coding of faces. Technical Report 317, MIT Media Lab Vismod, 1995.
9. H.A. Rowley, S. Baluja, and T. Kanade. Human face detection in visual scenes. In David S. Touretzky, Michael C. Mozer, and Michael E. Hasselmo, editors, *Advances in Neural Information Processing Systems*, volume 8, pages 875–881. The MIT Press, 1996.
10. A. Samal and P. Iyengar. Automatic recognition and analysis of human faces and facial expressions: A survey. *Pattern Recognition*, 8:65–77, 1992.
11. C. Tomasi and T. Kanade. Detection and tracking of point features. Technical Report CMU-CS-91-132, Carnegie Mellon University, 1991.
12. M. Turk and A. Pentland. Eigenfaces for recognition. *Journal of Cognitive Neuroscience*, 3(1):71–86, März 1991.
13. A. Wilson, C.L. Wilson, S. Sirohey, and C.S. Barnes. Human and machine recognition of faces: A survey. Technical Report CS-TR-3339, University of Maryland, College Park, August 1994.
14. L. Wiskott. Phantom faces for face analysis. In *Proc. IEEE Intern. Conf. on Image Processing, ICIP'97, Santa Barbara*, pages III 308–311. IEEE, October 1997.
15. G. Yang and T.S. Huang. Finding human faces in a picture. *Lecture Notes in Computer Science*, 719:766–773, 1993.
16. Alan L. Yuille, Peter W. Hallinan, and David C. Cohen. Feature extraction from faces using deformable templates. *International Journal of Computer Vision*, 8:99–111, 1992.